HAL
open science

Intergranular Corrosion of 2024 Alloy in Chloride Solutions

Christel Augustin, Eric Andrieu, Christine Blanc, Georges Mankowski, Jérôme Delfosse

To cite this version:

Christel Augustin, Eric Andrieu, Christine Blanc, Georges Mankowski, Jérôme Delfosse. Intergranular Corrosion of 2024 Alloy in Chloride Solutions. Journal of The Electrochemical Society, 2007, vol. 154, pp.C637-C644. 10.1149/1.2778224 . hal-00806063

HAL Id: hal-00806063

https://hal.science/hal-00806063v1

Submitted on 29 Mar 2013

HAL is a multi-disciplinary open access archive for the deposit and dissemination of scientific research documents, whether they are published or not. The documents may come from teaching and research institutions in France or abroad, or from public or private research centers.

L'archive ouverte pluridisciplinaire **HAL**, est destinée au dépôt et à la diffusion de documents scientifiques de niveau recherche, publiés ou non, émanant des établissements d'enseignement et de recherche français ou étrangers, des laboratoires publics ou privés.

Open Archive Toulouse Archive Ouverte (OATAO)
OATAO is an open access repository that collects the work of Toulouse researchers and makes it freely available over the web where possible.

This is an author-deposited version published in: http://oatao.univ-toulouse.fr/
Eprints ID : 2427

To link to this article :
URL : http://dx.doi.org/10.1149/1.2778224

To cite this version : Augustin, Christel and Andrieu, Eric and Blanc, Christine and Mankowski, Georges and Delfosse, Jérôme (2007) *Intergranular Corrosion of 2024 Alloy in Chloride Solutions.* Journal of The Electrochemical Society (JES), vol. 154 (n° 11). C637-C644. ISSN 0013-4651

Any correspondence concerning this service should be sent to the repository administrator: staff-oatao@inp-toulouse.fr

Intergranular Corrosion of 2024 Alloy in Chloride Solutions

Christel Augustin,[a] Eric Andrieu,[a] Christine Blanc,[a,*,z] Georges Mankowski,[a] and Jérôme Delfosse[b]

[a]*CIRIMAT, UMR CNRS 5085, ENSIACET, 31077 Toulouse Cedex 04, France*
[b]*EADS Innovation Works–IW/MS/MM, 92152 Suresnes Cedex, France*

Experiments were performed to determine the propagation kinetics of intergranular corrosion on 2024 aluminum alloy immersed in 1 and 3 M chloride solutions. Tests consisting of immersion in a corrosive solution followed by optical observations on sectioned samples were carried out. This method was found to be time consuming and led to a lack of reproducibility due to the random nature of the corrosion attacks. Another method proved to be more efficient; it consisted of measuring the load to failure on precorroded tensile specimens vs preimmersion time in an aggressive environment. This method was found to allow the mean depth of the corrosion defects to be determined. Further, in 1 and 3 M chloride solution, intergranular corrosion led to the formation of a nonbearing zone, the thickness of which was equal to the mean depth of the corrosion defects. This corroded zone explained the premature failure of the specimens when a uniaxial tensile stress was applied.
[DOI: 10.1149/1.2778224]

High strength aluminum alloys such as those of the 2xxx series are widely used in the aeronautical industry because of their low density and high specific strength. But, these alloys are susceptible to localized corrosion in chloride media such as pitting corrosion,[1,2] intergranular corrosion,[3,4] exfoliation,[5] and stress corrosion cracking.[6,7]

The localized corrosion sites are found in different locations on aircraft (fuselage skin, for example). Currently, zero damage is demanded; it means that all the corrosion damage detected is repaired, which implies high maintenance costs. To reduce these costs, alternative solutions are under study; one is to determine the growth kinetics of the corrosion damage so as to optimize the maintenance procedure of the aircraft structures affected.

Pitting and intergranular corrosion (IGC) susceptibility of 2xxx series Al alloys have been studied for decades.[3,8-10] IGC starts with the dissolution of the *S* phase particles (Al_2CuMg) on grain boundaries caused by the galvanic couples solute-depleted zone/surrounding matrix and solute-depleted zone/*S* phase particles.[11] Subsequently, IGC propagates by the dissolution of the copper-depleted zone along the grain boundaries.[12]

Many authors have determined the kinetics of IGC damage growth using different methods. Zhang and Frankel used the foil penetration technique to measure the time for the fastest-growing localized corrosion site to penetrate foils of various thicknesses.[13,14] They highlighted different kinetics of damage, considering the direction of growth, as a consequence of the microstructural anisotropy (slower kinetics in the short transverse direction). Moreover, they enriched this study with the development of a statistical model to predict the anisotropy of IGC kinetics and the effects of microstructure.[15]

In situ X-ray radiography was used by Zhao et al. to characterize IGC and exfoliation in high-strength Al alloys.[4] They found that growth kinetics for IGC sites are slower than those determined by the foil penetration technique. In situ X-ray radiography not only considers the fastest growing site but also takes a wide range of growth kinetics into account. Microfocal X-ray radiography was also used to characterize the transition from intergranular corrosion to intergranular stress corrosion cracking.[16]

To determine the kinetics of sharp IGC cracks in AA7178,[17] Huang and Frankel developed an approach based on sectioning and visual observations. Their method provides the growth rate of long sharp IGC cracks and not only the rates of the fastest growing sites.

The above methods do have their limitations. For example, sectioning does not take into account the three-dimensional (3D) morphology of the damage. Furthermore, there is no information about which parameter is the most damaging, the fastest growing defect or the average depth of all the growing defects.

This article presents an approach to characterize the IGC susceptibility of alloy 2024 T351 in chloride media. The method used, based on the decrease of the mechanical properties of precorroded specimens, has been successfully used by Garat et al. to study the intergranular oxidation damage on a nickel-based superalloy.[18] In the present study, this method provides results on the role of the nonbearing zone. Results are compared to those obtained with classical immersion and sectioning tests.

Experimental

Materials.— A 2024 T351 rolled plate (wt %: Cu 4.50%, Mg 1.44%, Mn 0.60%, Si 0.06%, Fe 0.13%, Zn 0.02%, and Ti 0.03%) 50 mm thick was provided by EADS. The T351 temper is obtained by solid-solution heat-treatment at 495°C (±5°C), water quenching, straining and tempering at room temperature for four days. To reveal the microstructure, electrochemical etching was performed followed by observations with an optical microscope. The specimen was mechanically polished with up to 4000 grit SiC papers and to 1 μm with diamond paste on the three principal faces (Fig. 1). Electrochemical etching was then conducted with HBF_4 (3.5 vol %) in distilled water (96.5 vol %) for 80 s (twice 40 s) under 20 V at room temperature. Examination was performed with an optical microscope under polarized light. The three main directions are referred to as *L* (longitudinal), *LT* (long transverse) and *ST* (short transverse). Figure 1 illustrates the elongated grain structure of the

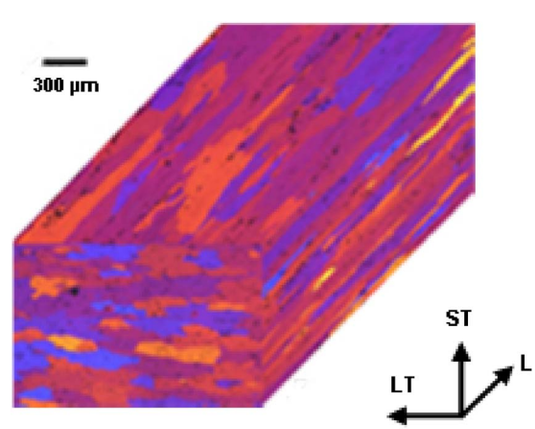

Figure 1. (Color online) Optical observation of a 2024 T351 rolled plate after mechanical polishing and electrochemical etching.

* Electrochemical Society Active Member.
z E-mail: christine.blanc@ensiacet.fr

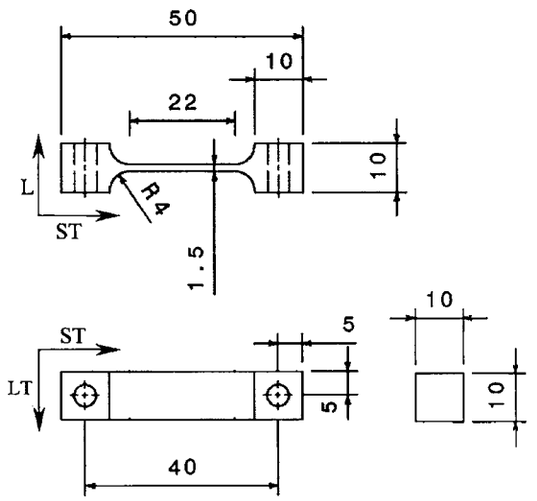

Figure 2. Tensile specimens for immersion test (all dimensions in mm).

2024 T351 rolled plate. The average grain sizes in the *L*, *LT*, and *ST* directions are, respectively, 700, 300, and 100 μm. In addition, second-phase particles such as Al_2CuMg (*S* phase particles) and Al–Cu–Mn–Fe particles, can be distinguished. Complementary transmission electron microscopy examinations revealed the presence of dispersoids ($Al_{20}Mn_3Cu$) in the matrix and Al_2CuMg particles on grain boundaries in good agreement with the literature.[11]

Intergranular corrosion tests.— In this study, two types of sample were used. First, cubic samples (10 × 10 × 10 mm) machined in the 2024 T351 plate were degreased in ethanol; then the faces perpendicular to the corrosion damage growing direction (*L*, *LT*, and *ST* directions) were mechanically polished with up to 4000 grit SiC paper in water, followed by ultrasonic cleaning in ethanol and air drying. Second, tensile specimens were machined from the plate thickness using conventional methods. Figure 2 presents the dimensions and the characteristic directions of the tensile specimens. Previous to any exposure to an aggressive solution, the sample surfaces were prepared following the same procedure as for the cubic samples.

Both types of sample (cubic and tensile specimens) were then exposed to NaCl solutions at two different concentrations (1 and 3 M). The first chloride solution (1 M) corresponds to a classic chloride content for intergranular corrosion tests. A higher chloride content was also used to reproduce what happens during alternate immersion and emersion periods (or drying effects) which lead to highly concentrated chloride solutions. The solution temperature was maintained at 25 ± 2°C assisted by a thermostated water bath. Exposure time varied from 12 h to seven days. After immersion, the samples were ultrasonically cleaned in ethanol, air dried, and stored in a desiccator.

Cubic samples were then sectioned with a diamond disk cutter perpendicularly to the corroded faces as explained in Fig. 3. The cross sections were examined by optical microscopy after being mechanically polished with up to 4000 grit SiC papers and with diamond paste up to 1 μm.

Tensile tests.— For the tensile tests, a 30 kN Instron 3367 testing machine was used. Displacement rate was imposed so that the strain rate was close to 10^{-3} s^{-1}. The mechanical properties which were considered during the test are the load and the strain to failure. In the present case, the load is more relevant than the stress since the tensile specimens were not considered as volume elements of continuum mechanics but as damaged structural elements. The tests led up to the failure of the tensile specimens stressed along the *ST* direction. Ten uncorroded tensile samples were tested to establish the reference curve.

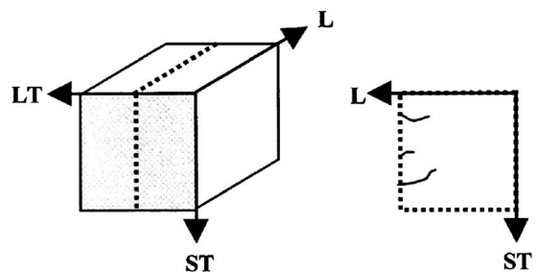

Figure 3. Notation and configuration for an immersion sample. The shaded area corresponds to the polished and corroded face.

Current-potential curves.— The tests consisted of the potentiokinetic polarization of the samples from the cathodic potential of −900 mV/saturated calomel electrode (SCE) to the highest potential of −400 mV/SCE. The potential sweep rate was 500 mV h^{-1}. All potentials quoted are relative to the saturated calomel electrode. The counter electrode was platinum. Before polarization, the specimen was mechanically polished with up to 4000 grit SiC papers and to 1 μm with diamond paste.

Results and Discussion

Preliminary tests.— Figure 4 shows a current-potential curve plotted for 2024 aluminum alloy in 1 M NaCl solution. The exposed surface corresponded to the *LT-ST* plane. The curve only exhibited one breakdown potential corresponding to the corrosion potential at −0.68 V/SCE. Optical observations of the electrode after the experiments showed that this breakdown potential was related to localized corrosion on 2024 aluminum alloy, i.e., pitting corrosion and intergranular corrosion. In the cathodic part, the curve presented a well-defined plateau for a current density of 5.10^{-5} A cm^{-2} corresponding to cathodic oxygen reduction.

These results thus proved that the 2024 alloy used in this study, immersed at the corrosion potential in 1 M NaCl solution, was susceptible to intergranular corrosion. Additional experiments were performed to compare the current-potential curves obtained for the two other planes of the plate with that obtained for the *LT-ST* plane.

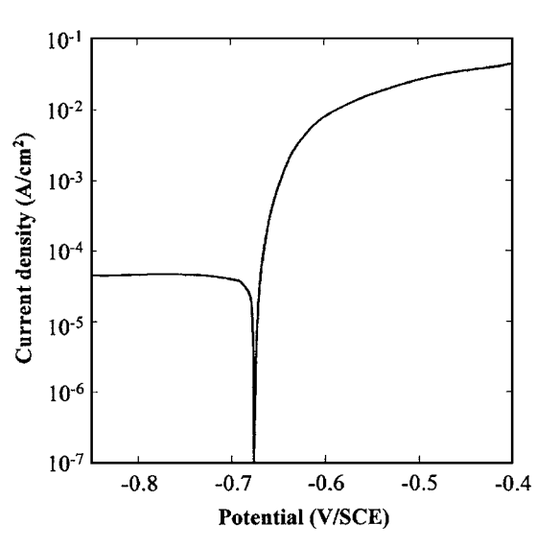

Figure 4. Current-potential curve for a 2024 T351 alloy sample (*LT-ST* plane) in a 1 M NaCl solution (T = 25°C).

Reproducibility of the different curves was checked and the results did not show any differences between the three planes. Thus, for these experimental conditions, plotting the current-potential curves did not allow the susceptibility to intergranular corrosion of the three characteristic planes of the rolled plate to be distinguished. Furthermore, the results were compared to those obtained by Guillaumin and Mankowski.[11] For the same experimental conditions, but for another batch, they showed that the current-potential curves revealed two breakdown potentials, one related to dissolution of *S*-phase particles and the other one to pitting and intergranular corrosion. Zhang and Frankel also observed two breakdown potentials on the current-potential curves plotted for 2024 alloy in chloride solutions: the first breakdown potential was related to *S*-phase dissolution as reported by Guillaumin and Mankowski but the second one was only related to intergranular corrosion.[12] Guillaumin and Mankowski also showed that the shape of the current-potential curves, i.e., the number of breakdown potentials, was related to the surface area of the sample.[11] With a very small area, they only observed one breakdown potential. Indeed, they showed that, on a given sample, not all the particles reacted at the same time. With a small area, due to the low number of particles, the anodic current related to *S*-phase dissolution was very low and thus only one breakdown potential was observed. Hence, it can be assumed that the differences between the results presented here and those obtained by Guillaumin and Mankowski were related to the volumic fraction of *S*-phase particles in the material.

Intergranular immersion tests.— Immersion tests were performed on cubic samples to study the propagation kinetics of intergranular corrosion in 2024 alloy. After immersion, the samples were sectioned and observed by means of an optical microscope. Figures 5a-c show optical micrographs obtained on 2024 alloy after different immersion times, i.e. 24, 72, and 168 h in 1 M NaCl solution. Intergranular corrosion was observed on all samples. Comparison between these micrographs shows that propagation of intergranular corrosion corresponded not only to an increase of the depth of the corrosion attacks but also to an increase of the width of the attacks which was confirmed by scanning electron microscopy observations (Fig. 5d). After 168 h, the size of the defect observed on the micrograph was 300 μm in depth and more than 50 μm in width. For a given experimental condition, such observations were performed on at least four sections to take into account problems related to the random nature of the corrosion process (Fig. 3). All the corrosion attacks were counted and their depths measured. Consequently, this allowed a statistical approach to be performed: for each experimental condition, the distribution of the depths of the corrosion defects was plotted. Two types of representation were studied: the first represented the cumulative probability vs the depth of the corrosion defects and the second the cumulative probability vs the logarithm of the depth of the corrosion defects. Figure 6 shows an example of such distributions obtained for samples immersed for seven days in 1 M NaCl. Figure 6a showed that the cumulative probability did not vary linearly with the depth of the corrosion defects while a linear variation was observed in the second case (Fig. 6b). Whatever the experimental conditions, the same observations were made. As a consequence, the average depth of the corrosion defects had to be calculated by considering the logarithm of the depth for all defects. Furthermore, extrapolation of the straight line observed in Fig. 6b for a probability of 100% allowed the maximum depth of the corrosion defects to be estimated. Figures 7-9 show the average depth, the maximum depth and the average density, respectively, of intergranular corrosion defects vs immersion time in 1 and 3 M NaCl solutions. The average depth of the corrosion defects was calculated as explained previously. For the maximum depth of the corrosion defects, estimated values from the distributions were compared to values resulting from the observations of the different sections, the depth of all defects observed on the different sections being measured. The defect density was related to the number of grain boundaries involved; it was expressed as the ratio between the number of grain boundaries actually corroded and the number of grain boundaries present. Figure 7 shows that the average depth of the corrosion defects increased as the immersion time in chloride solution increased for both chloride concentrations. No significant difference was observed between the values obtained in a 1 M chloride solution and those in 3 M chloride solution. In both cases, the average depth of the corrosion defects seemed to stabilize after 168 h of immersion, close to a value of 140 μm. For both concentrations, the values obtained after 72 h of immersion seemed to be too high by comparison to the others. This was related to the random nature of the corrosion attacks and probably to the random nature of their initiation time. Similarly, Fig. 8 shows that the maximum depth of the corrosion defects observed increased strongly in 3 M chloride solution as the immersion time increased, from a value of 275 μm after 12 h of immersion to a value of 750 μm after 168 h. In 1 M chloride solution, the maximum depth of the corrosion defects also increased as the immersion time increased but did not exceed a value of 500 μm. Comparison of measured values of the maximum depth with the values estimated from the distributions showed that there was a good agreement between the two sets of values (only the estimated value in 1 M NaCl solution after 72 h of immersion seemed to be incorrect). Problems related to the random nature of

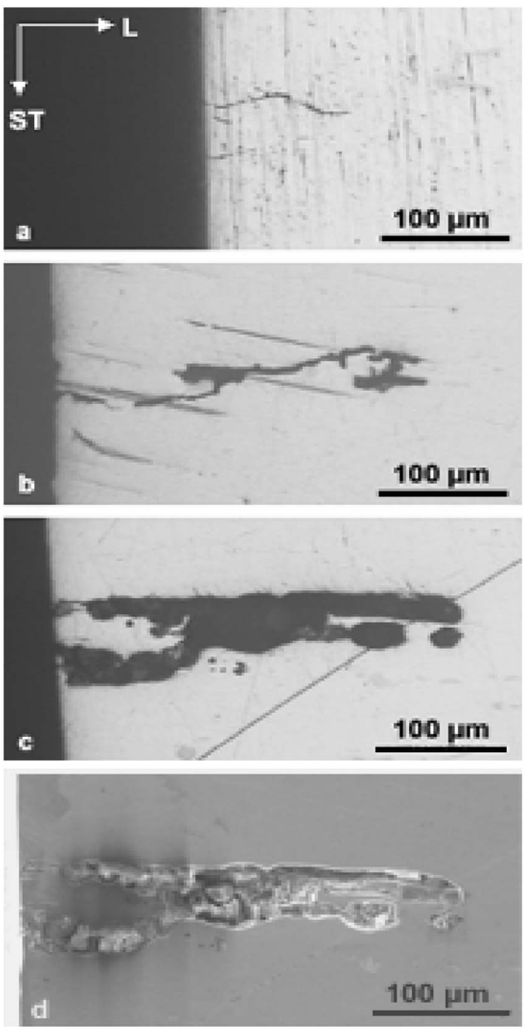

Figure 5. Intergranular corrosion defects observed on 2024 T351 alloy after immersion in 1 M NaCl solutions for (a) 24, (b) 72, and (c) 168 h at 25°C using an optical microscope. (d) SEM observations of intergranular corrosion defects observed after immersion for 168 h.

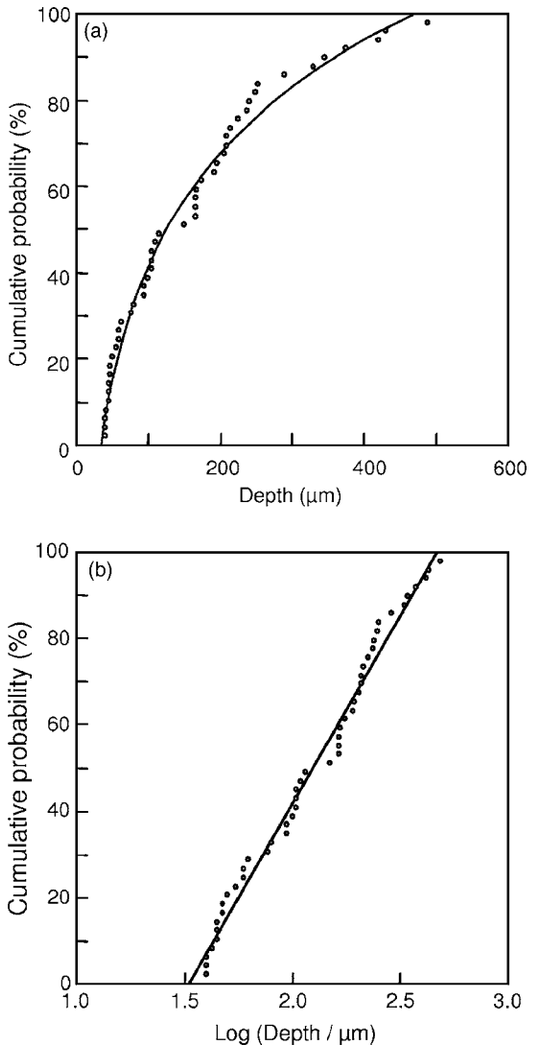

Figure 6. Cumulative probability vs (a) the depth and (b) the logarithm of the depth of intergranular corrosion defects in 2024 T351 alloy after seven days of immersion in 1 M NaCl solutions at 25°C (*L* direction).

the corrosion attack are also observed in Fig. 9 for a 1 M chloride concentration: the density of damage sites increased irregularly as the immersion time increased in 1 M chloride solution while, for a 3 M chloride solution, the average density of corrosion defects increased more regularly as the immersion time increased. The results thus show that determining the propagation kinetics of intergranular corrosion by sectioning and observing precorroded specimens needs a statistical approach due to the random nature of the corrosion attacks and thus the lack of reproducibility of the results. This is highly time consuming. Here, at least four sections were systematically analyzed which corresponded to extensive experimental work but even this was not enough. Further, Fig. 10 shows an optical micrograph of an AA2024 *LT-ST* plane after 24 h of immersion in 1 M NaCl. Numerous intergranular corrosion sites were observed over the whole surface. Particular attention was paid to three of them in order to study the geometry of the corrosion defects. Optical observations of these attacks were performed after different steps of polishing to accurately determine their depth: a 15 μm step and even sometimes less was selected. Figure 11 shows optical observations of one corrosion defect after polishing periods corresponding to different amounts of material removed, i.e., a removed thickness from 2 to 600 μm. Comparison of micrographs e and f shows that

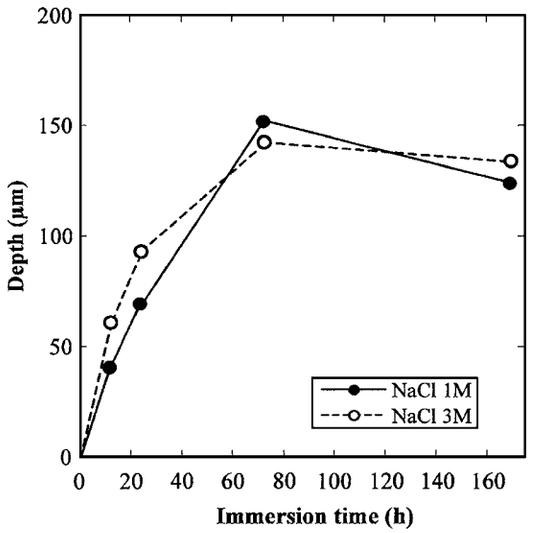

Figure 7. Average depth of intergranular damage in 2024 T351 alloy (*L* direction) after different immersion times in 1 and 3 M NaCl solutions at 25°C.

the maximum depth of this corrosion defect was around 600 μm since on micrograph f, some attacked grain boundaries are still visible. In Fig. 8, the maximum corrosion depth for a one-day immersion in 1 M NaCl was only 150 μm. This result confirms that determining the propagation kinetics of intergranular defects by sectioning and observing precorroded samples requires a very large number of samples to be observed. Such a method is thus highly time consuming and, with a reasonable number of samples, it allows only descriptive results to be obtained. In addition, it does not allow the 3D structure of the corrosion defects to be considered.

Tensile tests.— Tensile specimens were dimensioned, taking into account the previous results, in order for intergranular corrosion to lead to a significant effect on the mechanical properties of the specimens. Figure 12 shows the maximum load and the strain to failure of specimens precorroded during different immersion times in 1 or 3 M chloride solution. For each experimental condition, three ten-

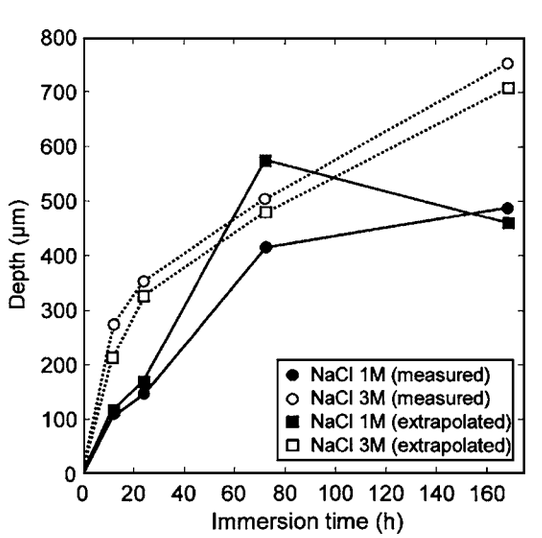

Figure 8. Maximal depth of intergranular corrosion damage in 2024 T351 alloy (*L* direction) after different immersion times in 1 M NaCl and 3 M NaCl solutions at 25°C.

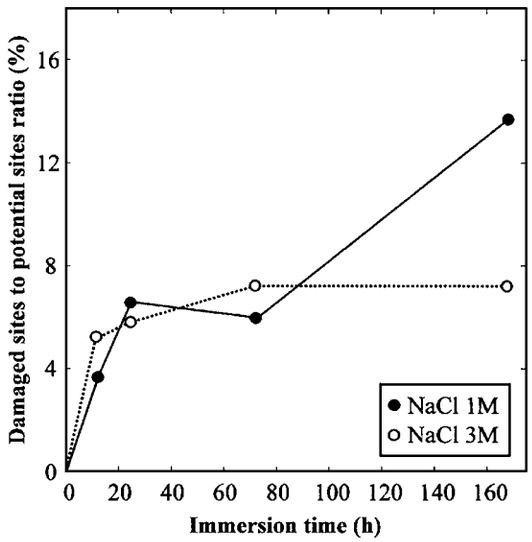

Figure 9. Ratio of damaged sites to potential sites for 2024 T351 alloy (*L* direction) after different immersion times in 1 M NaCl and 3 M NaCl solutions at 25°C.

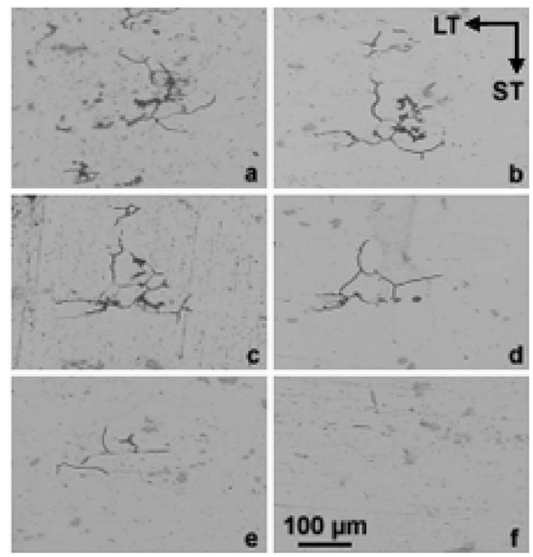

Figure 11. Three-dimensional description of an intergranular corrosion defect in 2024 T351 alloy (LT-ST face) after 24 h of immersion in a 1 M NaCl solution at 25°C. The sample was mechanically polished to progressively remove (a) 2, (b) 70, (c) 120, (d) 240, (e) 460, (f) 600 µm.

sile specimens were precorroded and then submitted to a tensile test. Figure 12a shows that, for both chloride concentrations, the load to failure significantly decreased as the immersion time increased. The choice for the dimensions of the tensile specimens proved to be suitable since immersion for 24 h in 1 M chloride solution led to a load to failure decrease from 6.5 kN for a noncorroded specimen to 5.4 kN for this corroded sample. For both concentrations, the load to failure decreased significantly during the first 24 h and then more slowly which was well correlated with the variation of the mean depth or the maximum depth of the corrosion defects vs immersion time shown in Fig. 7 and 8. Comparison of the results obtained for the two chloride concentrations shows also that, whatever the immersion time, the load to failure for a specimen immersed in 3 M chloride solution was lower than that for a specimen immersed in 1 M chloride solution. This strongly suggested that, for a given immersion time, intergranular corrosion, seen as the mean depth of the corrosion affected zone, propagated faster in 3 M chloride solution than in 1 M solution even though similar observations had not been made with sectioned samples. In parallel, Fig. 12b shows that immersion in chloride solution also rapidly led to a decrease in the strain to failure from 14.5% for a noncorroded specimen to 4.5%

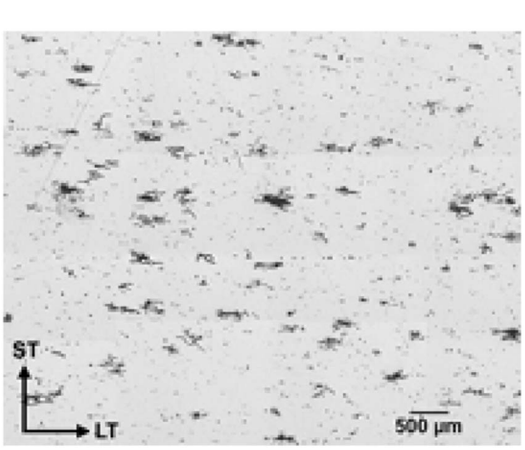

Figure 10. A corroded LT-ST face on 2024 T351 alloy after 24 h of immersion in a 1 M NaCl solution at 25°C.

after immersion for 168 h in 3 M chloride solution. The influence of the chloride content on the susceptibility to intergranular corrosion was again shown with strain to failure values lower for 3 M chloride than for 1 M chloride whatever the immersion time.

The present results thus showed that immersion in chloride solution induced a significant decrease of the mechanical properties of the 2024 alloy. Comparison of Fig. 12a and b showed that the strain to failure decreased more rapidly as the immersion time increased than the maximum load. This suggests the existence of a critical length for the intergranular corrosion defects corresponding to a reduced ductility for AA2024 alloy. Other authors obtained similar results. Pantelakis et al. showed that, after immersion in different aggressive solutions such as ASTM G110-92, a decrease of the ultimate stress and of the strain to failure was observed for various aluminum alloys such as 2024 alloy by comparison to results obtained on reference samples.[19] They also showed that the mechanical properties decreased as the immersion time increased following a nonlinear law. Furthermore, Petroyiannis et al. showed that the decrease of the ductility of 2024 alloy was attributed not only to the depth of the corroded zone, but also to the embrittlement induced by the hydrogen penetration.[20] But, the question now was to determine how homogeneously the corrosion damage was distributed in the tensile specimens. It was seen in Fig. 10 that corrosion defects seemed to be homogeneously distributed over the whole surface of the cubic sample. Furthermore, comparison of the load/strain curves obtained for an uncorroded specimen and for a specimen immersed for 72 h in a 1 M chloride solution showed that, even though the load and the strain were lower for the corroded specimens, the general shape of the curves was similar with no necking observed in either case (Fig. 13). The same results were obtained whatever the immersion test conditions. Observations of the tensile specimens after failure confirmed that there was no localization of deformation during the tensile tests (Fig. 14). Further, Fig. 14 showed that the corrosion damage was homogeneously distributed over the whole surface of the tensile specimen which is in good agreement with the very homogeneous distribution of corrosion damage observed in Fig. 10. It was thus assumed that, from a mechanical point of view, intergranular corrosion led to the presence in the material of a nonbearing zone. As the effective bearing area is decreased, the load to failure for a corroded specimen will decrease too. Following this assumption, the propagation of intergranular corrosion can be con-

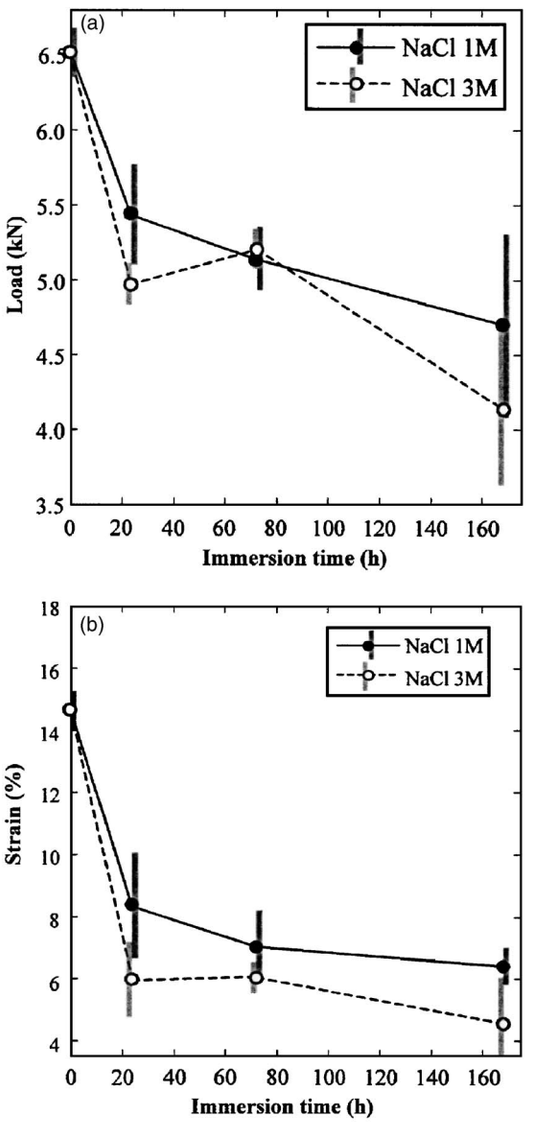

Figure 12. Evolution of (a) the maximum load and (b) the strain to failure for 2024 T351 tensile specimens corroded in 1 and 3 M NaCl solutions for different times at 25°C.

sidered as the growth of the thickness of the nonbearing zone along the whole length of the tensile specimens. Figure 15 gives a description of this approach: due to specimen geometry, the decrease of the bearing area was assumed to be essentially related to the propagation of intergranular corrosion on the large sides of the section. From this description of the corrosion damage and the results given in Fig. 12, it was then possible to calculate the thickness of the corroded zone, called $x(t)$, vs the time of immersion in chloride solution. As a consequence of this type of approach, it was assumed that the stress to failure σ_{fail} (ultimate stress) was a constant characteristic of the material. Thus, for an uncorroded specimen, this constant is given by the following equation

$$\sigma_{fail} = L_{fail}/(ba) = \text{constant} \quad [1]$$

where L_{fail} was the maximum load to failure and a and b were the dimensions of the tensile specimen as given in Fig. 2.

For a corroded specimen, the equation became

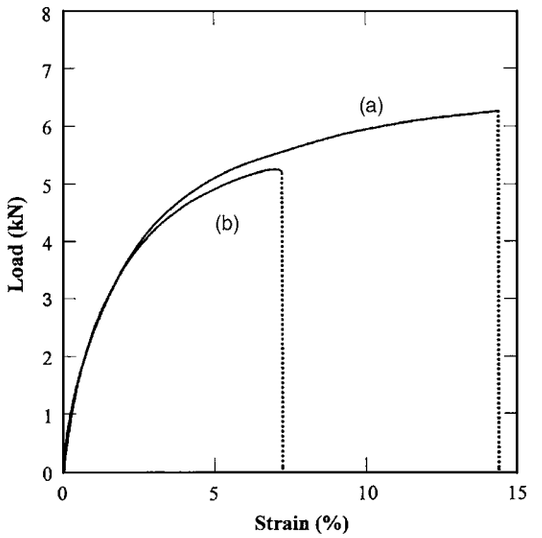

Figure 13. Load/strain curves for (a) an uncorroded 2024 T351 alloy sample and (b) a 2024 T351 alloy sample after 72 h of immersion in a 1 M NaCl solution at 25°C.

$$\sigma_{fail} = L_{fail}(t)/[b(a - 2x(t))] \quad [2]$$

where $L_{fail}(t)$ was the maximum load to failure measured for a precorroded specimen (t = immersion time). As $x(t)$ was negligible compared to the dimensions of the tensile specimens, the following equation was obtained

$$x(t) = [1 - (L_{fail}(t)/L_{fail})](a/2) \quad [3]$$

Figure 16 shows the depth of the corrosion defects, $x(t)$, for samples immersed in 1 and 3 M chloride solutions, calculated from the load vs immersion time curve (Fig. 12). For both concentrations, the depth of the corrosion defects increased as the immersion time in-

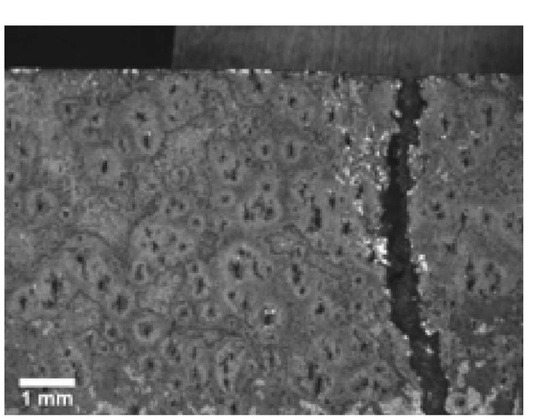

Figure 14. Observation of a 2024 T351 tensile specimen after failure. The specimen had been corroded in a 1 M NaCl solution for seven days at 25°C.

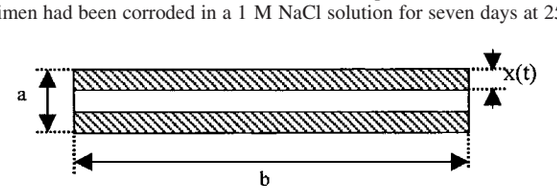

Figure 15. Section of a tensile specimen after immersion in a NaCl solution. The shaded area corresponds to the corroded zones [thickness $x(t)$ varying with immersion time].

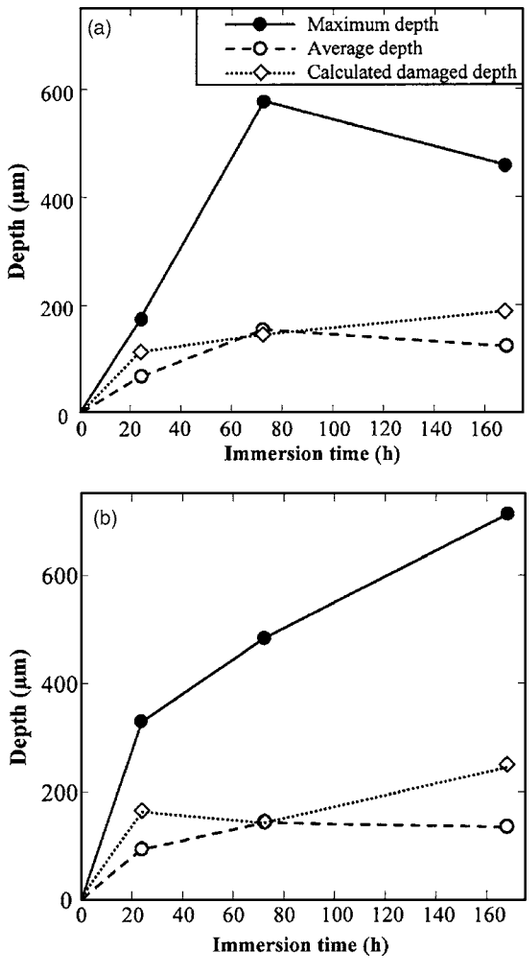

Figure 16. Maximum depth, average depth and calculated damaged depth of 2024 T351 alloy samples immersed in (a) 1 M and (b) 3 M NaCl solutions for different immersion times at 25°C.

creased. The fact that values obtained in 3 M chloride solution were slightly higher than those in 1 M chloride solution was attributed to the increased aggressiveness of the former solution. The curves showing the maximum measured depth and the average depth of the corrosion defects vs immersion time calculated with cubic samples (Fig. 7 and 8) are also reported in Fig. 16. It was demonstrated that, for both concentrations, there was a good agreement between the depth of the corrosion defects calculated from the tensile experiments and the mean depth calculated by sectioning immersed samples. These results thus showed first that it was possible to determine the propagation kinetics of intergranular corrosion using a method which was less time consuming than the conventional approach based on observations of sectioned samples after immersion tests. This method consisted of measuring the decrease of the mechanical properties (maximum load to failure) of precorroded tensile specimens vs immersion time in the aggressive solution. In addition, these results also indicated that the corrosion defects which induced the mechanical failure of the specimens during a uniaxial tensile test corresponded to the mean damage. In service, when a corroded part is submitted to uniaxial mechanical loading (tensile), the mean depth of the intergranular corrosion defects previously propagated corresponds to a dead zone. This leads to a decrease of the bearing area of the structural part and thus to a premature failure. The results shown in Fig. 16 suggest that defects with a depth greater than the mean depth did not have a significant effect on the mechanical behavior of the damaged specimens with uniaxial mechanical loading. To con-

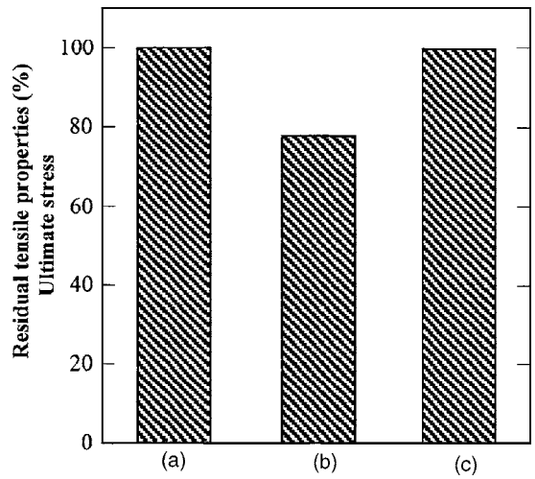

Figure 17. Degradation of tensile properties after immersion in 1 M NaCl solutions at 25°C, (a) uncorroded specimen as reference, (b) specimen after 24 h of immersion and (c) specimen after 24 h of immersion and polishing off of the corroded zones.

firm this assertion, additional experiments were performed using the same approach. Tensile specimens were precorroded in a 1 M chloride solution for 24 h. They were then polished to remove a thickness equal to the corroded zone and finally submitted to a tensile test. Tensile tests were also performed on uncorroded specimens. Figure 17 presents the results obtained after the tensile tests on uncorroded and corroded specimens. Results obtained on specimens corroded for 24 h in 1 M chloride solution are superimposed for comparison. Figure 17 shows the measured ultimate stress for the three types of sample. This value was expressed using the apparent section and not the effective section of the specimen; for an uncorroded specimen, the two values are the same but, for a corroded specimen for which the corroded zone was not removed, the effective section was equal to the apparent section minus the nonbearing zone affected by intergranular corrosion. The ultimate stress was significantly reduced for a corroded specimen by comparison to an uncorroded one. When the corroded zone was removed, a complete recovery of the measured ultimate stress occurred, confirming the previous interpretation. These observations are in agreement with results obtained by Pantelakis et al.[19] Furthermore, a partial recovery of the strain to failure (only 51.9% of the value obtained for the noncorroded specimen) after the removal of the corroded zone was also observed. This reduced ductility was attributed, as said previously and as shown by Petroyiannis et al., to the embrittlement induced by the hydrogen penetration.[20] The next step would be to determine, with more complex mechanical loading, the parameters relevant for damage (mean depth, maximum depth, or density of defects) which have to be considered in failure analysis of structural elements.

Conclusion

Experiments were performed to determine the propagation kinetics of intergranular corrosion on 2024 aluminum alloy immersed in chloride solutions. The tests consisted of immersion in corrosive solution followed by sectioning and observation of the samples using optical microscopy. The method was found to be time consuming and led to a lack of reproducibility due to the random nature of the corrosion attacks. Another method proved to be more efficient: it consisted of measuring the load to failure on precorroded tensile specimens vs immersion time in an aggressive environment. The results showed that this method allowed the mean depth of the corrosion defects to be determined. Moreover, in 1 and 3 M chloride solution, intergranular corrosion led to the growth of a nonbearing zone the thickness of which was equal to the mean depth of the

corrosion defects. This corroded zone explained the premature failure of the specimens when uniaxial tensile stress was applied.

Acknowledgments

This work was supported by EADS CCR France and DGA.

Centre National de la Recherche Scientific assisted in meeting the publication costs of this article.

References

1. Z. Szklarska-Smialowska, *Corros. Sci.*, **41**, 1743 (1999).
2. J. W. J. Silva, A. G. Bustamante, E. N. Codaro, R. Z. Nakazato, and L. R. O. Hein, *Appl. Surf. Sci.*, **236**, 356 (2004).
3. A. Garner and D. Tromans, *Corrosion (Houston)*, **35**, 55 (1979).
4. X. Zhao, G. S. Frankel, B. Zoofan, and S. Rokhlin, *Corrosion (Houston)*, **59**, 1012 (2003).
5. M. Posada, L. E. Murr, C. S. Niou, D. Roberson, D. Little, R. Arrowood, and D. George, *Mater. Charact.*, **38**, 259 (1997).
6. M. R. Bayoumi, *Eng. Fract. Mech.*, **54**, 879 (1996).
7. X. Liu, G. S. Frankel, B. Zoofan, and S. Rokhlin, *Corros. Sci.*, **49**, 139 (2007).
8. I. L. Muller and J. R. Galvele, *Corros. Sci.*, **17**, 179 (1977).
9. J. F. Li, Z. Ziqiao, J. Na, and T. Chengyu, *Mater. Chem. Phys.*, **91**, 325 (2005).
10. J. Galvele and S. De Micheli, *Corros. Sci.*, **10**, 795 (1970).
11. V. Guillaumin and G. Mankowski, *Corros. Sci.*, **41**, 421 (1998).
12. W. Zhang and G. S. Frankel, *Electrochim. Acta*, **48**, 1193 (2003).
13. W. Zhang and G. S. Frankel, *Electrochem. Solid-State Lett.*, **3**, 268 (2000).
14. W. Zhang and G. S. Frankel, *J. Electrochem. Soc.*, **149**, 510 (2002).
15. W. Zhang, S. Ruan, D. A. Wolfe and G. S. Frankel, *Corros. Sci.*, **45**, 353 (2003).
16. X. Liu, G. S. Frankel, B. Zoofan, and S. Rokhlin, *J. Electrochem. Soc.*, **153**, 42 (2006).
17. T. Huang and G. S. Frankel, *Corros. Sci.*, **49**, 858 (2007).
18. V. Garat, O. Brucelle, J. M. Cloue, V. Rebeyrolle, D. Monceau, B. Viguier, and E. Andrieu, *Mater. Sci. Forum*, **461–464**, 537 (2004).
19. Sp. G. Pantelakis, P. G. Daglaras, and Ch. Alk. Apostolopoulos, *Theor. Appl. Fract. Mech.*, **33**, 117 (2000).
20. P. V. Petroyiannis, Al. Th. Kermanidis, P. Papanikos, and Sp. G. Pantelakis, *Theor. Appl. Fract. Mech.*, **41**, 173 (2004).